Eur. Phys. J. B **12**, 525–540 (1999)

THE EUROPEAN PHYSICAL JOURNAL B

EDP Sciences

Cooperativity in a spin transition ferrous polymer: Interacting domain model, thermodynamic, optical and EPR study

C. Cantin, J. Kliava[a], A. Marbeuf, and D. Mikaïlitchenko

Centre de Physique Moléculaire Optique et Hertzienne[b], 351 Cours de la Libération, 33405 Talence Cedex, France

Received 27 November 1998 and Received in final form 19 April 1999

Abstract. A new thermodynamic model is proposed in order to account for the high spin ↔ low spin conversion in metal-organic polymers. The model, based on the idea that the spin conversion occurs in interacting domains of like-spin metal ions, allows to explain most of the important features of various types of spin conversion. The *sine qua non* condition of the existence of spin transitions with hysteresis is obtained. In the case of very large cooperativity, the model predicts unusual behaviour of the spin conversion system due to a low-temperature metastable high spin state. Existence of such a state is interesting in the context of the light induced excited spin state trapping recently observed in some ferrous compounds. The model is applied to interpret the spin transition in polycrystalline ferrous polymer $[Fe_{1-y}Cu_y(Htrz)_2trz](BF_4)$ with $y = 0.00, 0.01$ and 0.10, detected by differential scanning calorimetry, optical reflectivity and electron paramagnetic resonance. The domain size and the interaction energy between the domains are estimated as, respectively, $n = 11$ and $\Gamma = 2.010$ kJ mol^{-1} for the $y = 0$ compound. As the copper content is growing, n and Γ tend to decrease, resulting in transformations of the shape of hysteresis loop which becomes less steep, narrows and shifts to lower temperatures. The electron paramagnetic resonance gives further evidence of the presence of like-spin domains.

PACS. 65.50.+m Thermodynamic properties and entropy – 78.40.Me Organic compounds and polymers – 76.30.Fc Iron group ($3d$) ions and impurities (Ti–Cu)

1 Introduction

In octahedral ligand fields, transition metal ions with d^4, d^5, d^6 or d^7 configurations adopt either a high spin (HS) or a low spin (LS) electronic arrangement, according to whether the cubic crystal-field splitting $10Dq$ is lower or higher than the mean spin pairing energy P. When these two energies are comparable, a spin conversion can be induced under the influence of temperature, pressure, or by irradiating with light. For the purposes of the advanced technology, most interesting are spin transition compounds showing bistability behaviour on the microscopic scale [1], resulting in abrupt spin transitions with a large thermal hysteresis. This explains the increasing interest to the Fe^{2+}–4–R–1, 2, 4-triazole compounds during the last decade [2]. Owing to an associated thermochromic effect, such compounds can be used as molecular-based memory devices and displays.

The cooperative character of the spin transitions has been discussed by several authors in terms of electron-phonon coupling, cooperative Jahn-Teller interaction between the HS ions or elastic interaction between ions in different spin states [3].

If cooperativity between spin-changing complexes is weak, gradual spin conversion is observed over an extended temperature range. In contrast, in systems with strong cooperativity abrupt conversion may occur, often accompanied by hysteresis and structural changes. In the latter case the term "spin transition" is used.

The spin conversion is likely to start from a growth of nucleation centres of a new spin state, probably localised at defect sites, grain boundaries and on the surface of crystallites. Strong cooperative interactions favour the growing of *domains* of like-spin ions from these nuclei, resulting in an abrupt transition. In contrast, weak cooperative interactions impede the nucleation centres to achieve a critical size required for the development of domains [4]. The existence of like-spin domains has been clearly demonstrated by grinding and doping spin transition compounds [5,6]. The more gradual conversion observed has been related to decrease of domain size caused by crystal defects.

Thermodynamic analysis provides a very convenient way for characterising the spin conversion, as far the latter is accompanied by a change of entropy and volume which both increase in the HS state. Thus, from the thermodynamic point of view, the driving force of the spin conversion is the difference in the Gibbs free energy

[a] e-mail: jkliava@frbdx11.cribx1.u-bordeaux.fr
[b] UMR Université Bordeaux I-CNRS 5798

between the two spin states involved. The analysis of this difference allows to predict the relative stability of these states and evaluate the fundamental physical characteristics of the spin conversion.

In this work, a new thermodynamic model is developed, taking into account the existence of *interacting* LS and HS domains. The model allows not only to explain most of the important features of spin conversion, but also it predicts for the first time the existence in some cases of metastable high spin states in the low-temperature range. Of a particular interest may be the possibility of populating such states by the light-induced excited spin state trapping (LIESST).

For definiteness, we consider the case of ferrous ions, though the model can be applied to any spin-changing ion. The interacting domain model is further employed to interpret the spin transition with hysteresis in polymer ferrous compound $[Fe_{1-y}Cu_y(Htrz)_2trz](BF_4)$ with $y = 0.00$, 0.01 and 0.10. The predictions of the thermodynamic model are compared to the experimental results of differential scanning calorimetry (DSC), optical transmission and electron paramagnetic resonance (EPR) data. Computer simulations demonstrate that both the transition temperatures in cooling and warming modes and the slope of the hysteresis curve are correlated with the domain size. The influence of interdomain interaction energy is also studied, showing that the hysteresis loop vanishes not only for weak interactions, but also in the case of very strong interactions.

2 Interacting domain model

2.1 Theoretical description

As has been shown by Zimmermann and König [7], first-principle microscopic LS–HS conversion models in the Bragg-Williams or the molecular field approximations yield free-energy expressions explicitly taking into account interactions between HS and LS ions. These expressions are analogous to the one suggested by Slichter and Drickamer [8] in the framework of a phenomenological regular solution model of pressure-induced spin conversion. However, the latter authors consider randomly distributed HS or LS ions and *not* HS and LS domains. A thermodynamic model of spin conversion taking into account domains of like-spin ions has first been put forward by Sorai and Seki [9], however, they have only considered independent domains. This hypothesis is in contradiction with experimental studies showing that interaction between domains should take a prominent part in determining the behaviour of spin conversion systems [10]. The interacting domain case has been outlined by Purcell and Edwards [11].

The temperature-induced spin conversion being usually observed at constant pressure p and not at constant volume V, the appropriate thermodynamic potential is the Gibbs free energy (note however that in the solid state the pV term which distinguishes it from the Helmholtz free energy can usually be neglected).

We consider a one-mole sample of a metal-organic (ferrous) polymer in which the HS and LS molecules form linear domain chains of average length of l domains with exactly n molecules per domain. Only pairwise interactions between nearest neighbouring molecules are taken into account. At a temperature T, the sample contains D_{H} HS and D_{L} LS domains, the total number of domains per mole being $D = D_{\mathrm{H}} + D_{\mathrm{L}} = \mathcal{N}/n$, where $\mathcal{N}$ is the Avogadro's number. The Gibbs free energy of such a sample is given by

$$G_T = G_0 + G_{\mathrm{mix}} + G_{\mathrm{domains}} + G_{\mathrm{interchain}} \tag{1}$$

where G_0 is the contribution from *isolated* molecules or domains, G_{mix} is related to the mixing entropy S_{mix}, G_{domains} arises from molecule contacts inside the like-spin domains as well as from interdomain interactions on the chains, and $G_{\mathrm{interchain}}$ is due to molecule interactions between adjacent chains.

Let $x = D_{\mathrm{H}}/D$ be the HS molar fraction varying in the range $]0, 1[$. G_0 can be can be written as

$$G_0 = \mathcal{N}\left[x\gamma_{\mathrm{H}} + (1-x)\gamma_{\mathrm{L}}\right], \tag{2}$$

where the subscripts H and L refer to the low spin and high spin states, respectively, and γ_{H} and γ_{L} are one-molecule Gibbs energies.

In the actual case the mixing entropy is determined by the number of ways of distributing D_{H} HS and D_{L} LS domains within the assembly of D domains. In the Stirling approximation,

$$G_{\mathrm{mix}} = -TS_{\mathrm{mix}} = k_{\mathrm{B}}T \ln\left(D_{\mathrm{H}}^{D_{\mathrm{H}}} D_{\mathrm{L}}^{D_{\mathrm{L}}}/D^D\right), \tag{3}$$

or, as $D_{\mathrm{H}} = Dx$ and $D_{\mathrm{L}} = D(1-x)$,

$$G_{\mathrm{mix}} = \frac{\mathcal{N}k_{\mathrm{B}}}{n} T\left[x\ln x + (1-x)\ln(1-x)\right]. \tag{4}$$

The third term on the right-hand side of (1) can be written as

$$G_{\mathrm{domains}} = G^{\mathrm{intra}} + G^{\mathrm{inter}}, \tag{5}$$

where G^{intra} and G^{inter} account, respectively, for the contributions of intradomain contacts and interdomain contacts on the polymer chains. As noticed in [11], the interaction energies between the corresponding ions inside the like-spin domains and between two domains may be quite different. So, we denote these energies, respectively, as $\gamma^{\mathrm{i}}_{\mathrm{HH}}$, $\gamma^{\mathrm{i}}_{\mathrm{LL}}$ and $\gamma^{\mathrm{d}}_{\mathrm{HH}}$, $\gamma^{\mathrm{d}}_{\mathrm{LL}}$, $\gamma^{\mathrm{d}}_{\mathrm{HL}}$. The number of molecule contacts within a linear domain being $n-1$, we get

$$G^{\mathrm{intra}} = \mathcal{N}\left(1 - \frac{1}{n}\right)\left[x\gamma^{\mathrm{i}}_{\mathrm{HH}} + (1-x)\gamma^{\mathrm{i}}_{\mathrm{LL}}\right]. \tag{6}$$

In calculating the contribution from interdomain interactions, Purcell and Edwards [10] introduce an effective number of molecule pair contacts at the domain interface. However, as far as these authors neglect interchain interactions, at the actual stage this number must be taken

as one (in our approach these interactions are included in $G_{\text{interchain}}$). For a polymer chain containing on an average d_{H} HS and d_{L} LS domains with $d_{\text{H}} + d_{\text{L}} = d$, the numbers of different interdomain contacts i_{ij} are

$$i_{\text{HH}} = \frac{d_{\text{H}}(d_{\text{H}} - 1)}{d}, \quad i_{\text{LL}} = \frac{d_{\text{L}}(d_{\text{L}} - 1)}{d}, \quad i_{\text{HL}} = \frac{2d_{\text{H}}d_{\text{L}}}{d}\,. \tag{7}$$

The numbers I_{ij} of such interdomain contacts in the whole one-mole sample are obtained by multiplying the corresponding i_{ij} by the total number of chains, D/d. Thus,

$$G^{\text{inter}} = \frac{\mathcal{N}}{n}\left[x\left(x - \frac{1}{d}\right)\gamma^{\text{d}}_{\text{HH}} + (1-x) \times \left(1 - x - \frac{1}{d}\right)\gamma^{\text{d}}_{\text{LL}} + 2x(1-x)\gamma^{\text{d}}_{\text{HL}}\right]. \tag{8}$$

Finally, $G_{\text{interchain}}$ can be calculated by introducing a number of neighbouring chains, v ($v = 2$ and $v \geq 3$ for a two-dimensional and a three-dimensional structure, respectively). We assume that the interchain molecular interaction energies, noted as $\gamma^{\text{c}}_{\text{HH}}$, $\gamma^{\text{c}}_{\text{LL}}$ and $\gamma^{\text{c}}_{\text{HL}}$, are the same for the $\mathcal{N}(1 - 2/nd)$ non-terminating and $2\mathcal{N}/nd$ terminating molecules having, respectively, v and $v+1$ interchain contacts. The frequencies of the HH, LL and HL contacts being proportional, respectively, to x^2, $(1-x)^2$ and $2x(1-x)$, we get

$$G_{\text{interchain}} = \frac{1}{2}\mathcal{N}\left(v + \frac{2}{nd}\right) \times \left[x^2\gamma^{\text{c}}_{\text{HH}} + (1-x)^2\gamma^{\text{c}}_{\text{LL}} + 2x(1-x)\gamma^{\text{c}}_{\text{HL}}\right]. \tag{9}$$

Taking into account (2, 4, 6, 8, 9) results in

$$G_T(x) = xG_{\text{H}} + (1-x)G_{\text{L}} + rT\left[x\ln x + (1-x)\ln(1-x)\right] + \Gamma x(1-x), \tag{10}$$

where

$$\begin{cases} \dfrac{G_{\text{H}}}{\mathcal{N}} = \gamma_{\text{H}} + \left(1 - \dfrac{1}{n}\right)\gamma^{\text{i}}_{\text{HH}} + \dfrac{1}{n}\left(1 - \dfrac{1}{d}\right)\gamma^{\text{d}}_{\text{HH}} + \left(\dfrac{v}{2} + \dfrac{1}{nd}\right)\gamma^{\text{c}}_{\text{HH}}, \\ \dfrac{G_{\text{L}}}{\mathcal{N}} = \gamma_{\text{L}} + \left(1 - \dfrac{1}{n}\right)\gamma^{\text{i}}_{\text{LL}} + \dfrac{1}{n}\left(1 - \dfrac{1}{d}\right)\gamma^{\text{d}}_{\text{LL}} + \left(\dfrac{v}{2} + \dfrac{1}{nd}\right)\gamma^{\text{c}}_{\text{LL}}, \\ \dfrac{\Gamma}{\mathcal{N}} = \dfrac{1}{n}\left(2\gamma^{\text{d}}_{\text{HL}} - \gamma^{\text{d}}_{\text{HH}} - \gamma^{\text{d}}_{\text{LL}}\right) + \left(\dfrac{v}{2} + \dfrac{1}{nd}\right) \times \left(2\gamma^{\text{c}}_{\text{HL}} - \gamma^{\text{c}}_{\text{HH}} - \gamma^{\text{c}}_{\text{LL}}\right), \\ r = \dfrac{\mathcal{N}k_{\text{B}}}{n}. \end{cases} \tag{11}$$

Taking in (10) G_{L} as the origin of the energies,

$$G_T(x) = x\Delta H + T\{r[x\ln x + (1-x)\ln(1-x)] - x\Delta S\} + \Gamma x(1-x), \tag{12}$$

where ΔH and ΔS are the changes of the molar enthalpy and entropy associated with the LS to HS conversion ($\Delta G = \Delta H - T\Delta S$). In order to somewhat simplify the subsequent analysis, we assume Γ to be independent of temperature. At the particular temperature defined by $\Delta G = 0$,

$$T_{1/2} = \frac{\Delta H}{\Delta S}, \tag{13}$$

the $G_T(x)$ graph is symmetric with respect to $x = 1/2$.

As far as the Gibbs energies for isolated molecules can be assumed to be much greater than the intermolecular interaction energies, G_{H} and G_{L} in the first approximation are independent of n. In contrast, Γ and the corresponding "transition cooperativity" defined as $\Gamma/2RT_{1/2}$ [11], may well depend on the domain size. For very long chains, with $nd \gg 1$, the contribution to Γ from interchain interactions becomes independent on n. On the other hand, if one neglects interchain interactions, Γ will decrease with increasing n, unless the interdomain interaction energies, in turn, increase with n.

Stable or metastable equilibrium states of the system correspond to the minima of $G_T(x)$, while its maxima describe unstable equilibrium. The x-values corresponding to the extrema of $G_T(x)$ are obtained from the cancellation of the function $G'_T(x)$ given by

$$G'_T(x) = \Delta H + \Gamma(1-2x) - T\left(\Delta S + r\ln\frac{1-x}{x}\right). \tag{14}$$

This yields the implicit equation

$$\ln\frac{1-x}{x} = -\frac{2\Gamma}{rT}x + \frac{\Delta H - T\Delta S + \Gamma}{rT}\,. \tag{15}$$

The mathematical form of equation (14) is quite similar to that obtained in previous studies [8,11], however, the physical meaning of the parameters involved, see equation (11), is somewhat different.

For $x \to 0$ $G'_T(x) \to -\infty$ and for $x \to 1$ $G'_T(x) \to \infty$, so that equation (15) always has at least one solution. However, we are particularly interested in the cases of existence of more that one solution of this equation, since such cases result in bistability of the thermodynamic system which can manifest itself in the phenomenon of hysteresis. Note that in the present model metastable states, strictly speaking, have infinitely long lifetimes, since thermal fluctuations and tunneling through the free energy barrier are not taking into account. We will go back over this problem in the discussion (Sect. 5.1).

2.2 Graphical solution

The equation (15) can be solved by a graphical method. With this aim, we consider a plane (u, v) in which

Table 1. Characterisation of the regions I to VI by inequalities on Γ.

Region	Inequalities on Γ
I	$0 < \Gamma < \Delta H$ and $0 < \Gamma < 2rT_{1/2}$
II	$\Delta H < \Gamma < 2rT_{1/2}$
III	$2rT_{1/2} < \Gamma < \Delta H$
IV	$2rT_{1/2} < \Gamma < \Delta H \coth(\Delta S/2r)$ and $\Delta H < \Gamma < \Delta H \coth(\Delta S/2r)$
V	$\Gamma > \Delta H \coth(\Delta S/2r)$
VI	$\Gamma < 0$

the left-hand side and the right-hand side of equation (15) are represented, respectively, by a curve $(\mathcal{C})$ of equation $v = \ln[(1-u)/u]$ and a straight line (D_T) of slope $-2\Gamma/rT$. One can easily show that at any temperature (D_T) is passing through a fixed point P of coordinates $u_P = \frac{1}{2} + \Delta H/2\Gamma$ and $v_P = -\Delta S/r$. Then, provided that the quantities ΔH, ΔS and Γ are known, the x-values corresponding to the extrema of $G_T(x)$ can be determined from an intersection of $(\mathcal{C})$ and (D_T). The number of solutions will depend on the position of P.

The LS to HS conversion is always accompanied by an increase in entropy, $\Delta S > 0$. Indeed, in the HS state the electronic entropy is higher than in the LS state, because of greater spin degeneracy, and the vibrational entropy also is higher in the HS state, since weakening of metal-to-ligand bonds, accompanying the increase of ionic radius of the spin-changing ion, results in a higher density of vibrational states in comparison with the LS state. Therefore, only the cases of P located in the negative semi-plane $v < 0$ are physically meaningful.

Different types of behaviour of the thermodynamic system in question can be classified in accordance with the position of P inside the regions delimited by the curve $(\mathcal{C})$ $v = \ln[(1-u)/u]$, its inflexion tangent $v = -4u + 2$, its asymptote $u = 1$ and the straight line $u = 1/2$.

So, the negative semi-plane is subdivided into six regions numbered from I to VI, as shown in Figure 1. Expressing u and v *via* the thermodynamic parameters, each region can be characterised by inequalities on Γ, see Table 1.

From Figure 1 the following conclusions can be drawn.

(i) In the regions I and VI at any temperature there is only one intersection point between $(\mathcal{C})$ and (D_T).

(ii) In the regions II and V (D_T) can have three intersection points with $(\mathcal{C})$, case (a), provided its slope is sufficiently steep, $0 < T < T_B$ in the region II or $0 < T < T_A$ in the region V. The case (b), that of (D_T) tangent to $(\mathcal{C})$ for $T = T_B$ in the region II and $T = T_A$ in the region V, separates these temperature ranges from those of existence of only one solution, case (c), $T > T_{B,A}$. Note that in the regions II and V the abscissa of the tangency point lies above and below 0.5, respectively.

(iii) In the region III (D_T) is tangent to $(\mathcal{C})$ at two distinct temperatures, $T = T_B$ and $T = T_A$, respectively, cases (b) and (d). So, the implicit equation (15) has three different solutions inside the temperature range $T_B < T < T_A$.

(iv) In the region IV the situation is more complex, since there are three different temperatures, $T = T_{B_2}, T_{B_1}, T_A$, for which (D_T) is tangent to $(\mathcal{C})$, cases (b), (d), and (f). Therefore, equation (15) has three different solutions within two temperature ranges, $0 < T < T_{B_2}$ and $T_{B_1} < T < T_A$, cases (a) and (e).

2.3 Analytical approach

In order to discriminate between the roots of (15) corresponding to minima and maxima of $G_T(x)$, it is necessary to inspect its second derivative,

$$G''_T(x) = \frac{2\Gamma(x^2 - x + rT/2\Gamma)}{x(1-x)}, \tag{16}$$

in the range $]0,1[$.

For $\Gamma < 0$ G''_T is always positive. Neither can it be negative if $\Gamma > 0$ and $T \geq \Gamma/2r$, so that the implicit equation (15) always has only one solution in these cases.

More interesting is the case of $\Gamma > 0$ and $T < \Gamma/2r$, since the equation $G''_T(x) = 0$ has then two different roots, $x_- = \left(1 - \sqrt{\Delta}\right)/2 < 1/2$ and $x_+ = \left(1 + \sqrt{\Delta}\right)/2 > 1/2$, where $\Delta = 1 - 2rT/\Gamma$, so that the $x^2 - x + rT/2\Gamma$ polynom is negative within the range $x_- < x < x_+$ and positive elsewhere. Therefore, $G'_T(x)$ has a maximum at x_- and a minimum at x_+. In this case, the equation (15) has three different solutions if $G'_T(x_-) > 0$ and $G'_T(x_+) < 0$, two different solutions if either $G'_T(x_-) = 0$ or $G'_T(x_+) = 0$, and a single solution otherwise.

In order to determine the signs of the extrema of $G'_T(x)$, T is expressed in terms of x_- or x_+ from the condition that $G''_T(x) = 0$, as follows:

$$T = 2\Gamma(x_\pm - x_\pm^2)/r. \tag{17}$$

Inserting this relation in (14) yields a new one-argument function

$$G'_T(x) = \Delta H + \Gamma(1-2x) - 2\Gamma(x - x^2) \times \left(\frac{\Delta S}{r} + \ln\frac{1-x}{x}\right), \tag{18}$$

where $x = x_-$ or $x = x_+$, respectively for $0 < x < 1/2$ and $1/2 < x < 1$. $G'(x)$ represents the *locus of extrema* of $G'_T(x)$ at different temperatures.

The corresponding derivative,

$$G''(x) = -2\Gamma(1-2x)\left(\frac{\Delta S}{r} + \ln\frac{1-x}{x}\right), \tag{19}$$

is positive within the range of $1/2 < x < \frac{1}{2}[1 + \mathrm{th}(\Delta S/2r)]$ and negative elsewhere, see Table 2. Therefore, $G'(x)$ takes a minimum value of $\Delta H - \Gamma\Delta S/2r$ at $x = 1/2$ and

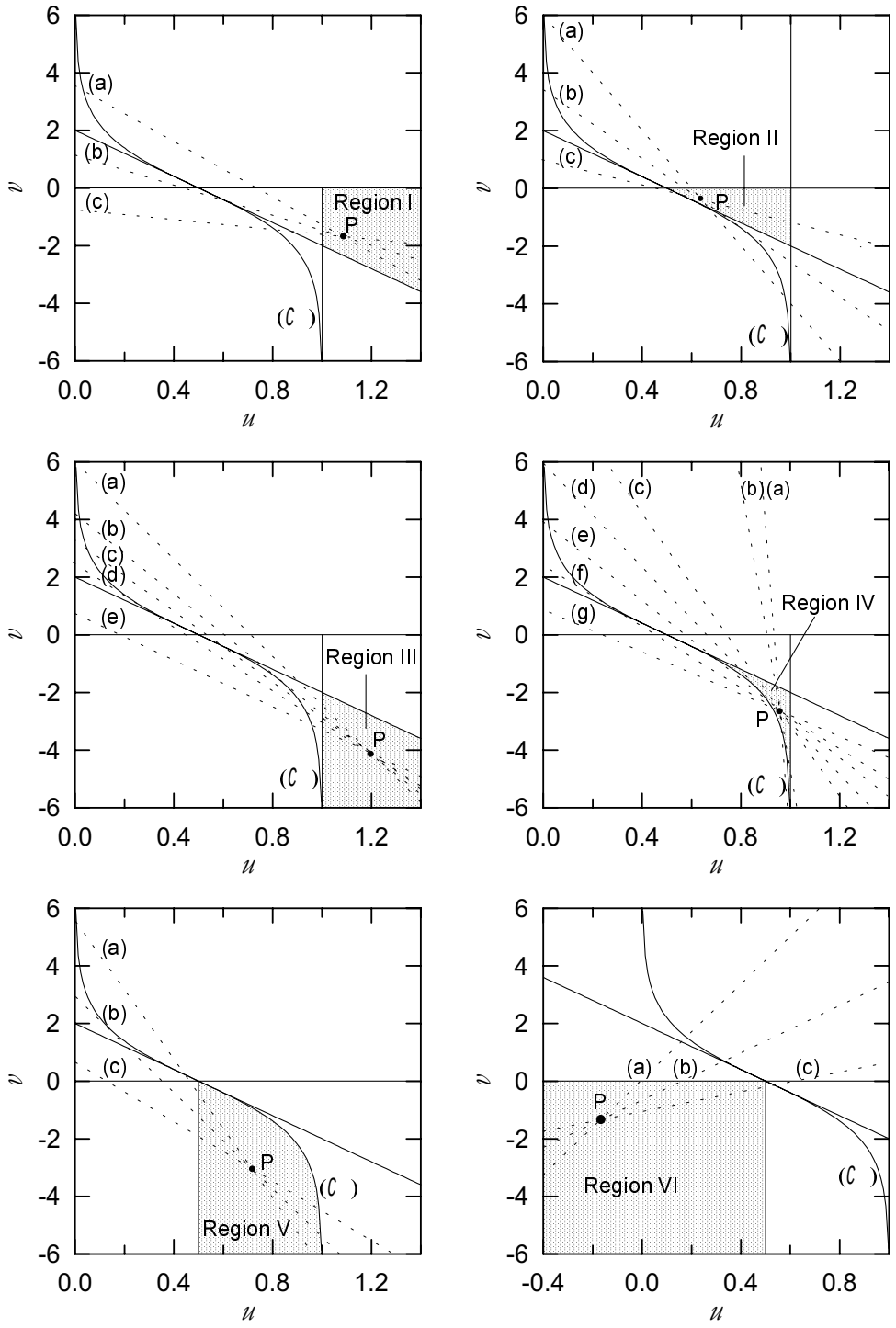

Fig. 1. Geometrical analysis of the number of intersection points, i, between the curve $v = \ln[(1-u)/u]$ ($\mathcal{C}$, solid) and the straight lines $v = [\Delta H + \Gamma(1-2u)]/rT - \Delta S/r$ (dotted). P is the fixed point. Region I: (a) $T < T_{1/2}$: $i = 1$; (b) $T = T_{1/2}$: $i = 1$; (c) $T > T_{1/2}$: $i = 1$. Region II: (a) $T < T_B$: $i = 3$; (b) $T = T_B$: $i = 2$; (c) $T > T_B$: $i = 1$. Region III: (a) $T < T_B$: $i = 1$; (b) $T = T_B$: $i = 2$; (c) $T_B < T < T_A$: $i = 3$; (d) $T = T_A$: $i = 2$; (e) $T > T_A$: $i = 1$. Region IV: (a) $T < T_{B_2}$: $i = 3$; (b) $T = T_{B_2}$: $i = 2$; (c) $T_{B_2} < T < T_{B_1}$: $i = 1$; (d) $T = T_{B_1}$: $i = 2$; (e) $T_{B_2} < T < T_A$: $i = 3$; (f) $T = T_A$: $i = 2$; (g) $T > T_A$: $i = 1$. Region V: (a) $T < T_A$: $i = 3$; (b) $T = T_A$: $i = 2$; (c) $T > T_A$: $i = 1$. Region VI: (a) $T < T_{1/2}$: $i = 1$; (b) $T = T_{1/2}$: $i = 1$; (c) $T > T_{1/2}$: $i = 1$.

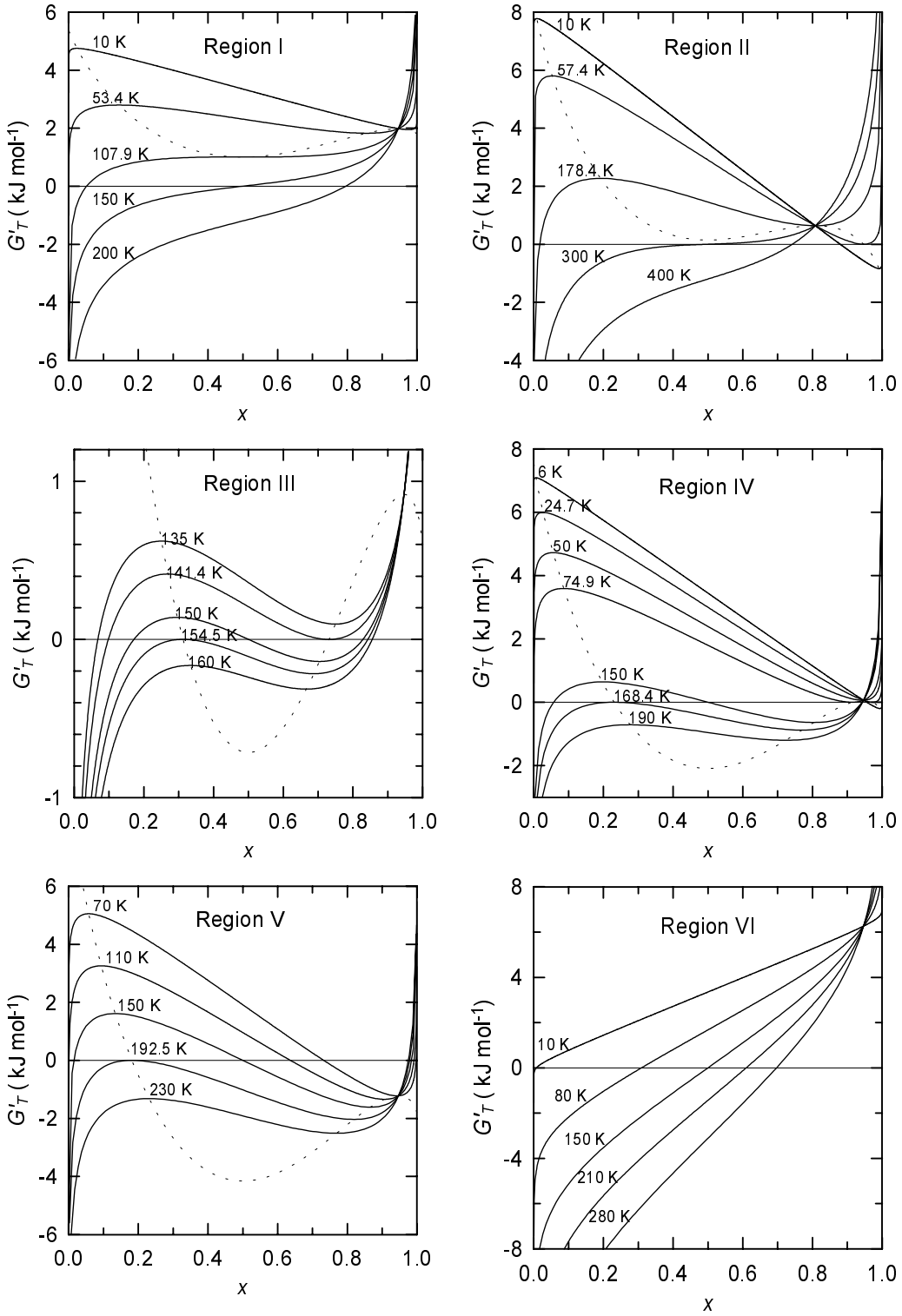

Fig. 2. Derivative of the molar Gibbs free energy *versus* the HS molar fraction. The values of ΔS are 24 $\mathrm{Jmol^{-1}\,K^{-1}}$ in all the regions, except for the region II, where 12 $\mathrm{Jmol^{-1}\,K^{-1}}$. The values of the interaction energy Γ are as follows (in $\mathrm{kJ\,mol^{-1}}$): region I, 1.79 ; region II, 4.78 ; region III, 2.99 ; region IV, 3.95 ; region V, 5.38 and region VI, -2.99. The dashed curves are the $G'(x)$ functions, see equation (18), representing the loci of extrema of $G'_T(x)$.

a maximum value of $\Delta H - \Gamma \mathrm{th}(\Delta S/2r)$ at $x_f = \frac{1}{2}[1 + \mathrm{th}(\Delta S/2r)]$. Note also that for $x = x_f$ the temperature dependence of $G'_T(x)$ vanishes, so that the set of $G'_T(x)$-curves for different temperatures has a common point of intersection of coordinates, x_f, $y_f = \Delta H - \Gamma \mathrm{th}(\Delta S/2r)$, see Figure 2.

Table 2. Variations of $G'(x)$ in the case $\Gamma > 0$ and $T < \Gamma/2r$. The T-values shown refer to the corresponding values of x_- and x_+ defined in equation (17).

	‖	x_-	‖		x_+		‖
x	0		1/2		$\frac{1}{2}[1+\tanh(\Delta S/2r)]$		1
$G''(x)$		−	0	+	0	−	
$G'(x)$	$\Delta H+\Gamma$	↘	$\Delta H-\Gamma\Delta S/2r$	↗	$\Delta H-\Gamma\tanh(\Delta S/2r)$	↘	$\Delta H-\Gamma$
T	0	↗	$\Gamma/2r$	↘	$\Gamma/[2r\coth^2(\Delta S/2r)]$	↘	0

Table 3. Signs of limiting and extreme values of $G'(x)$ in the different regions.

	Region I	Region II	Region III	Region IV	Region V
sign $(\Delta H+\Gamma)$	+	+	+	+	+
sign $(\Delta H-\Gamma\Delta S/2r)$	+	+	−	−	−
sign $[\Delta H-\Gamma\tanh(\Delta S/2r)]$	+	+	+	+	−
sign $(\Delta H-\Gamma)$	+	−	+	−	−

The limiting values of $G'(x)$ for $x \to 0$ and $x \to 1$ are $\Delta H+\Gamma$ and $\Delta H-\Gamma$, respectively. The signs of these values, shown in Table 3, unambiguously settle the signs of $G'_T(x_-)$ and $G'_T(x_+)$ in the six different regions.

Thus, the conclusions (i) to (iv) enumerated to the end of the previous section can be easily verified.

3 Computer simulations

In order to illustrate the behaviour of the thermodynamic system of interacting domains, we have carried out a computer analysis of the Gibbs free energy $G_T(x)$ and of its derivative $G'_T(x)$ *versus* the HS molar fraction x, as well as of x *versus* temperature T for each of the six regions specified in Section 2.2. The $x(T)$ graphs calculated from equation (15) by expressing T as a function of x,

$$T = \frac{\Delta H+\Gamma(1-2x)}{\Delta S + r\ln\dfrac{1-x}{x}}, \tag{20}$$

include both positive and negative temperatures. Branches shown by dashed lines correspond to physically non-accessible states of unstable equilibrium that is to maxima of $G_T(x)$.

In all the simulations given in this section, the value of $\Delta H = 3.60$ kJ mol^{-1} has been chosen in a somewhat arbitrary way. The ΔS- and Γ-values have been adjusted such as to satisfy the inequalities quoted in the Table 1 for the respective regions.

3.1 Absence of domains

At this stage, the number n of ions per domain has been fixed to one (individual ions). The $G'_T(x)$, $G_T(x)$ and $x(T)$ graphs for the six regions are shown respectively in Figures 2 to 4.

3.1.1 Region I

In this region $G'(x)$ does not go through zero, see the dashed curve for this region in Figure 2, therefore $G_T(x)$ has a single minimum. As the temperature increases, the position of the minimum gradually shifts from $x \approx 0$ to the right, reaching 0.5 for $T = T_{1/2}$ and approaching 1 at higher temperatures.

The corresponding $x(T)$ graph shows a gradual spin conversion. Note that in this case the *spin equilibrium* term is most appropriate.

3.1.2 Region II

One can see that $G'(x)$ takes a zero value corresponding to a minimum of $G'_T(x)$ in its tangency point with the x axis at $T = T_B = 57.4$ K. Below this temperature $G_T(x)$ has two minima, the lower one for x close to 0 and the higher one for x close to 1, corresponding, respectively to a stable LS state and to a metastable HS state. As T increases, the first minimum shifts to the right while the second one first shifts to the left and vanishes at $T = T_B$. For $T > T_B$ $G_T(x)$ has a single minimum which gradually shifts to higher x-values, so that the system is enriched in HS ions.

In the corresponding $x(T)$ graph, T_B represents a bifurcation point. If at low temperature the system is in the LS state, only a usual, gradual and reversible spin conversion is obtained. On the other hand, if the probability of "jumping" over or tunnelling through the free energy barrier is weak, the system can initially be trapped in the metastable HS state. In this case an irreversible HS to LS transition would occur, in addition, at $T = T_B$.

3.1.3 Region III

In this region, $G'(x)$ vanishes in two points, corresponding the first to a maximum and the second to a minimum of

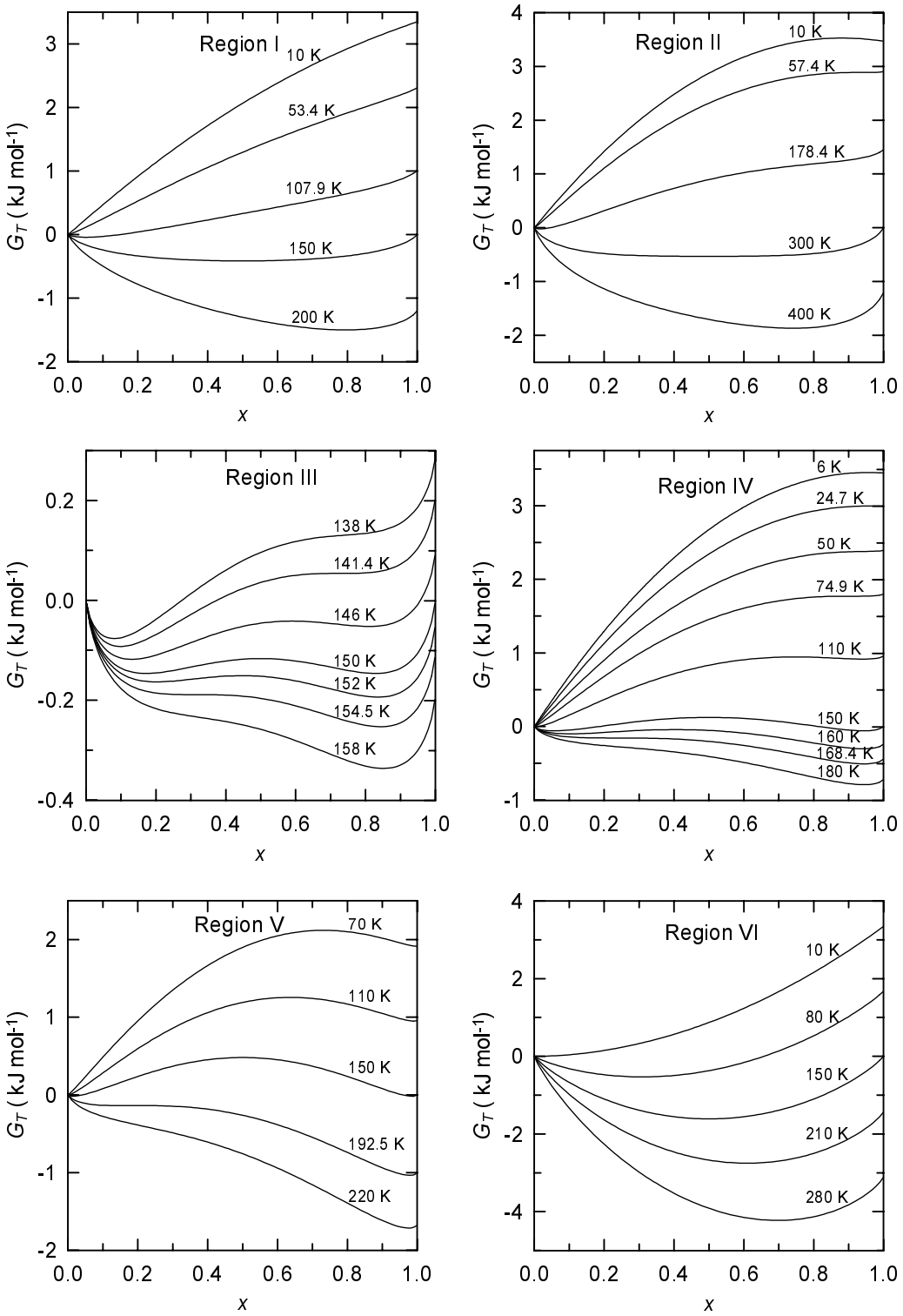

Fig. 3. Molar Gibbs free energy *versus* the HS molar fraction in the regions I to VI (see the legend of Fig. 2 for the thermodynamic parameters used).

$G'_T(x)$, respectively at $T = T_A = 154.5$ K and $T = T_B = 141.4$ K.

Inside the $T_B < T < T_A$ range G_T has two minima, the "LS" one for x closer to 0 and the "HS" one for x closer to 1. At $T = T_{1/2}$ the two minima are symmetrical with respect to $x = 0.5$ and have exactly the same energy. For $T_B < T < T_{1/2}$ the "LS" minimum corresponds to a stable state and the "HS" one to a metastable state, while for $T_{1/2} < T < T_A$ the situation is inverted. When the system is passing through $T_{1/2}$ in the warming mode,

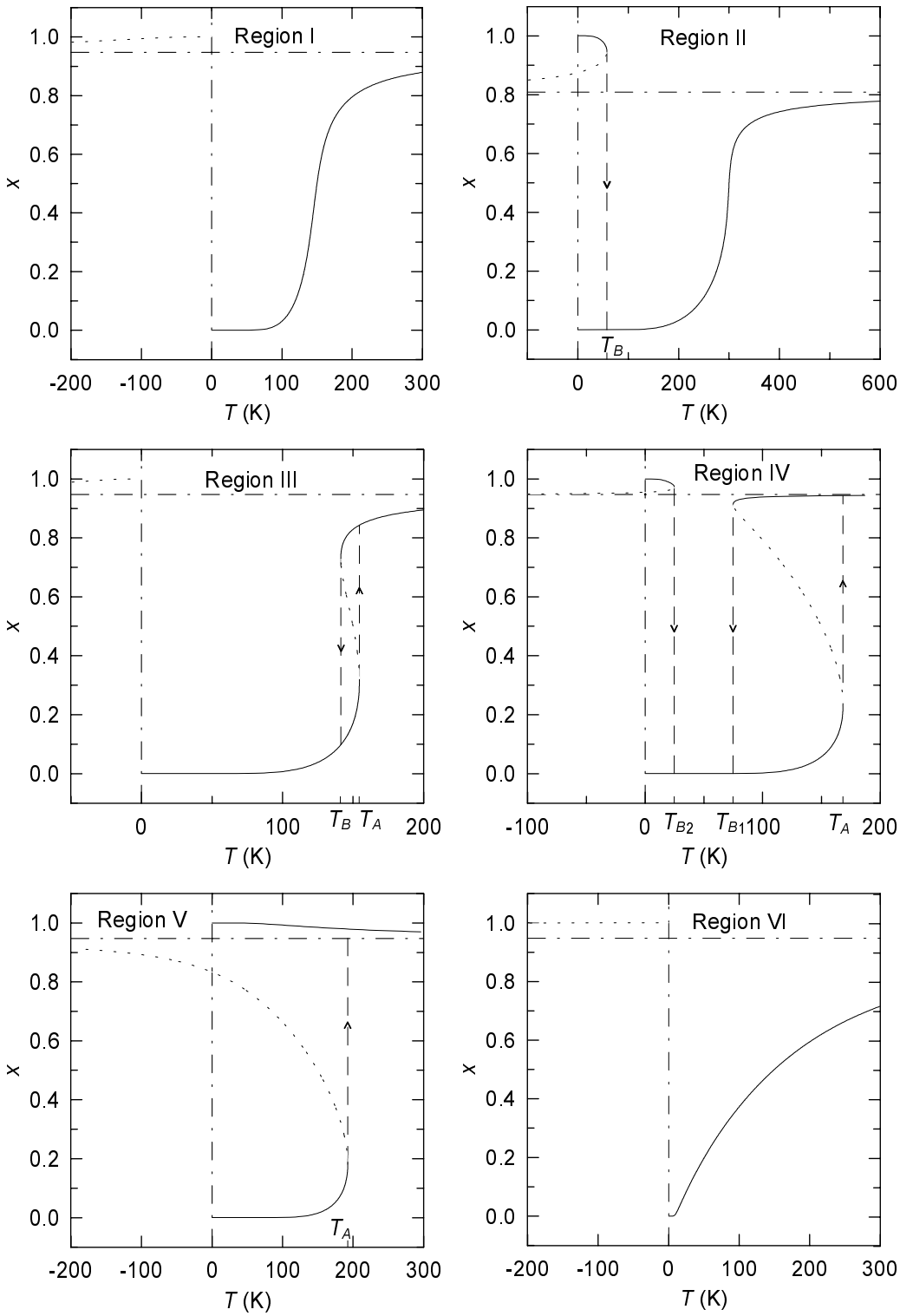

Fig. 4. HS molar fraction *versus* temperature in the regions I to VI (see the legend of Fig. 2 for the thermodynamic parameters used).

the "HS" minimum becomes thermodynamically stable. If the free energy barrier between the two minima were "transparent", the system would undergo the spin transition at this temperature. In the opposite case of totally impenetrable barrier, the system remains trapped in the now metastable "LS" minimum, until $T = T_A$ is reached. At the latter temperature, the barrier between the two minima disappears, so that the LS to HS transition finally takes place. Similarly, in the cooling mode, below $T_{1/2}$ the system can remain in the metastable "HS" minimum until

$T = T_B$, at which temperature it undergoes the HS to LS transition.

Outside the $T_B < T < T_A$ range $G_T(x)$ has only one minimum corresponding to a system rich in LS ions below T_B and in HS ions above T_A.

The $x(T)$ graph displays a spin transition with hysteresis with transition temperatures T_B and T_A, respectively in the cooling and warming modes.

3.1.4 Region IV

In this region the situation is more complex, since $G'(x)$ has three intersection points with the x-axis. The first one corresponds to a maximum of $G'_T(x)$ at $T_A = 168.4$ K and the second and third to minima of $G'_T(x)$ at $T_{B_1} = 74.9$ K and $T_{B_2} = 24.7$ K. Thus, there are two distinct temperature ranges, $T_{B_1} < T < T_A$ and $0 \leq T < T_{B_2}$, in which $G_T(x)$ has two minima. In the first range, the behaviour of the thermodynamic system is quite analogous to that in the region III, *vide ultra*. In the warming mode the LS to HS transition occurs at T_A, while in the cooling mode the HS state persists until the temperature is lowered down to T_{B_1}.

In contrast, in the $0 \leq T < T_{B_2}$ range, the minimum at $x \approx 1$ always corresponds to a metastable HS state, whereas the minimum at $x \approx 0$ is the stable LS state. If the system is initially in the HS state, a HS to LS transition will be observed at $T = T_{B_2}$, just as in region II. The corresponding $x(T)$ curve exhibits a spin transition with hysteresis that can be preceded by an irreversible HS to LS transition at T_{B_2}.

3.1.5 Region V

Here the situation is inverted with respect to the region II, namely, $G'(x)$ has one zero value corresponding to a maximum of $G'_T(x)$ at $T = T_A = 192.5$ K. From the $G_T(x)$ curves a somewhat unusual behaviour of the thermodynamic system is anticipated. At $T = 70$ K the LS minimum is lower in energy than the HS minimum and corresponds to a stable state. In raising the temperature, the energy difference between the two minima reduces and vanishes at $T = T_{1/2} = 150$ K. At still higher temperatures the HS minimum is lower in energy than the LS minimum but the system remains in the metastable LS state until $T = T_A$. At this temperature the LS minimum disappears and the LS to HS transition occurs. In contrast, in lowering the temperature, the system is "frozen" in the HS state, since the HS minimum never vanishes.

Otherwise, if the system initially founds itself at low temperature in the metastable HS state, no spin transition at all will be observed.

The $x(T)$ graph illustrates the two possible types of behaviour depending on the initial state of the spin system: an irreversible LS to HS spin transition at $T = T_A$ or absence of any spin transition. Note that the two bistabilities observed in the previous region collapse on the boundary between the regions IV and V, that is, for $\Gamma = \Delta H \coth(\Delta S/2r)$.

3.1.6 Region VI

Γ being negative in this region, $G'_T(x)$ monotonously increases with x. The $G_T(x)$ curves show a single minimum which smoothly shifts to the right as the temperature is increased. The $x(T)$ graph exhibits a very gradual spin conversion covering a large temperature range.

By inspecting the $x(T)$ graphs in the different regions, Figure 4, one general feature of the spin conversion can be deduced. Namely, all these graphs have a horizontal asymptote for a value of x defined by vanishing of the denominator in equation (20). Thus, the graphs always consist of two separate branches only discontinuous transitions being possible between them. Moreover, the asymptote prevents the spin system of reaching the 100% HS state at high temperatures, so that, strictly speaking, a spin conversion can never be complete.

3.2 Influence of the domain size

Now we shall demonstrate the influence of the domain size on the hysteresis cycle. We choose the region III, in which the bistability of the thermodynamic system manifests itself in the simplest way.

It has been established in Section 2.1, equation (11) that the parameter Γ and the transition cooperativity may depend on the domain size.

The $x(T)$ graphs corresponding to the case of Γ decreasing as n^{-1} are displayed in Figure 5 for different n values (we remind the reader that such a dependence is expected if interchain interactions can be neglected and interdomain interaction energies are independent of n). In this case, the hysteresis loop narrows with the increase in the domain size and disappears for a certain n value. On the other hand, the spin transition becomes more abrupt and more complete.

Figure 6 shows the behaviour of the spin transition system for Γ independent on n. This type of behaviour can be expected in metal-organic polymers with strong interchain interactions. Another possibility is that of interdomain interaction energies increasing with the domain size which may be the case if these energies are rather of elastic nature. In this instance, if the HS and LS ions are randomly distributed on the polymer chains ($n = 1$), a gradual spin conversion takes place. With the advent of even very small domains (of a size of a few molecules) a hysteresis loop emerges and broadens in a spectacular way as n increases. In addition, it becomes square-shaped, so that the spin transition is now very abrupt in both the warming and cooling modes. Practically no residual HS fraction at lower temperature or residual LS fraction at higher temperature is observed, so that the spin transition is almost complete.

Namely, one can see from the latter figure that with the chosen thermodynamic parameters the bistability occurs only due to the development of domains.

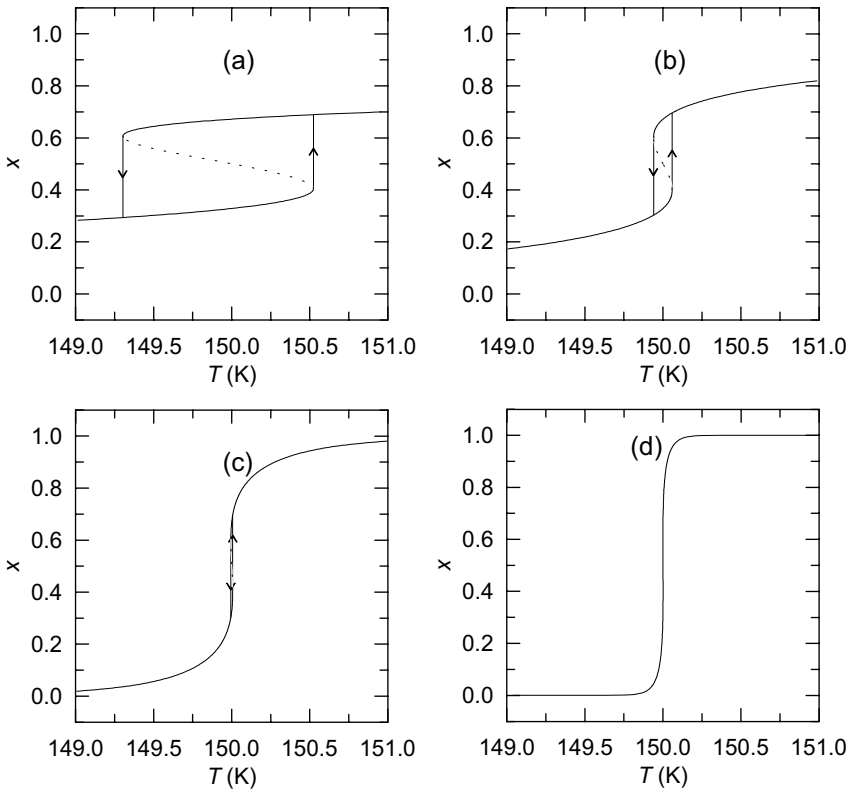

Fig. 5. HS molar fraction *versus* temperature plots for different domain size: $n = 1$ (a), 10 (b), 100 (c) and 1 000 (d). The remaining simulation parameters are: $\Delta H = 3.60$ kJ mol^{-1}, $\Delta S = 24$ J mol^{-1}K^{-1}, $n\Gamma = 2.60$ kJ mol^{-1}.

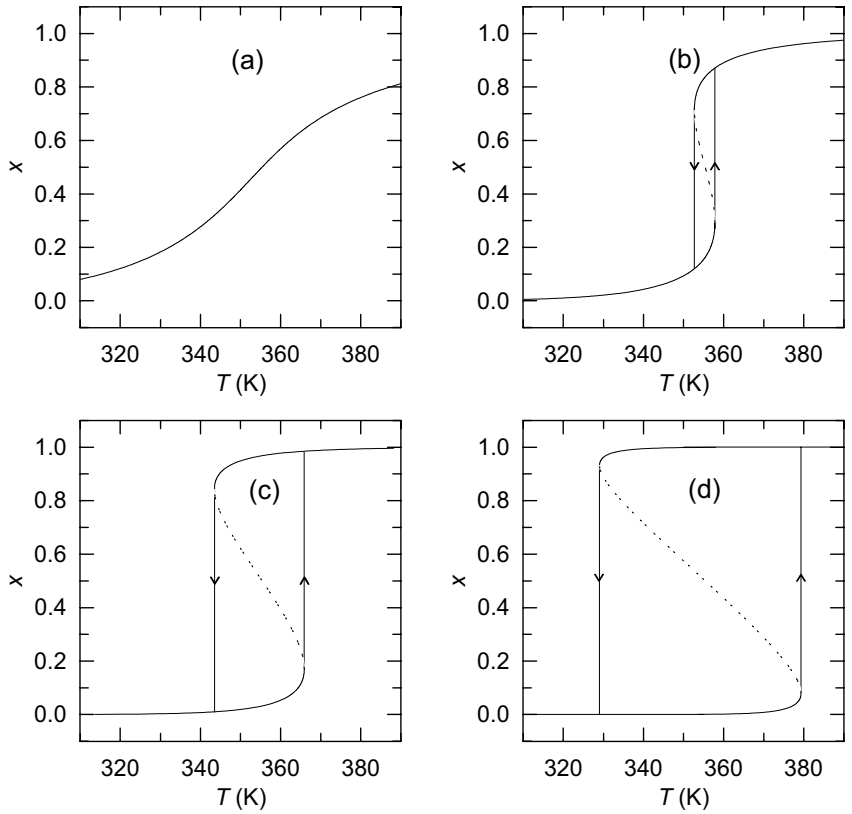

Fig. 6. HS molar fraction *versus* temperature plots for different domain size: $n = 1$ (a), 2 (b), 3 (c), and 6 (d). The remaining simulation parameters are: $\Delta H = 25.72$ kJ mol^{-1}, $\Delta S = 72.37$ J mol^{-1}K^{-1}, $\Gamma = 3.59$ kJ mol^{-1}.

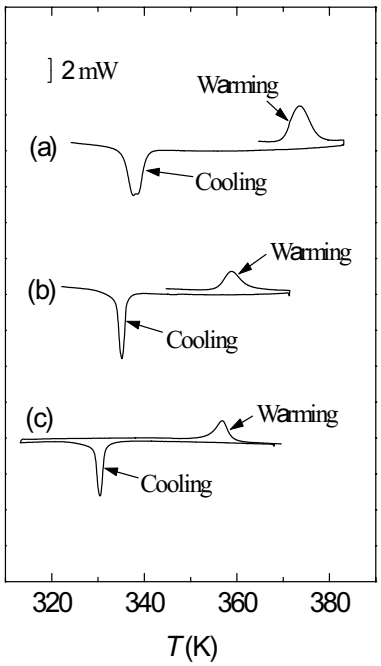

Fig. 7. Evolution of the DSC peaks in the warming and cooling modes in the $[Fe_{1-y}Cu_y(Htrz)_2trz](BF_4)$ compound for $y = 0.00$ (a), $y = 0.01$ (b) and $y = 0.10$ (c).

Table 4. Experimental (optical detection and DSC) values of the spin transition temperatures in the warming ($T_{1/2}\nearrow$) and cooling ($T_{1/2}\swarrow$) modes and model parameters in $[Fe_{1-y}Cu_y(Htrz)_2trz](BF_4)$ for different y values determined from DSC measurements (ΔH_{DSC}, ΔS_{DSC}) and computer fits ($\Delta H_{calc.}$, $\Delta S_{calc.}$, $\Gamma_{calc.}$, $n_{calc.}$). The numbers in brackets are errors in the last digits.

y	0.00	0.01	0.10
$T_{1/2}\nearrow$ (K) DSC	371(1)	356(2)	353(2)
$T_{1/2}\nearrow$ (K) optical	372(1)	357(1)	351(2)
$T_{1/2}\swarrow$ (K) DSC	343(2)	336(1)	333(2)
$T_{1/2}\swarrow$ (K) optical	343(1)	336(1)	334(2)
ΔH_{DSC} (kJ mol^{-1})	26.6(3)	15.9(4)	14.5(4)
$\Delta H_{calc.}$ (kJ mol^{-1})	26.50(6)	16.32(6)	14.96(6)
ΔS_{DSC} (Jmol^{-1} K^{-1})	72(1)	45(1)	41(1)
$\Delta S_{calc.}$ (Jmol^{-1} K^{-1})	74.2(2)	47.0(2)	43.7(2)
$\Gamma_{calc.}$ (kJ mol^{-1})	2.01(6)	1.76(6)	1.69(6)
$n_{calc.}$	11	7	6

4 Experimental section

Calorimetric measurements were made on the molecular compound $[Fe_{1-y}Cu_y(Htrz)_2trz](BF_4)$ for $y = 0.00, 0.01$ and 0.10, with a Perkin-Elmer DSC7 Differential Scanning Calorimeter (DSC) under the following conditions:

(i) temperature range between 310 and 390 K,
(ii) heating and cooling rates of 2 K/min,
(iii) sample mass of 4 mg,
(iv) four independent measurements for each composition.

The random errors in the temperatures as well as those in the heat effects derived from the DSC curves were obtained by the Student's method with 95% threshold of reliability. The systematic errors are estimated as 0.2 K and 2% in temperatures and heat effects, respectively. For all the compounds, the DSC curves, see Figure 7, show a positive peak in the warming mode and a negative one in the cooling mode at a lower temperature, confirming a thermally-induced Fe^{2+} spin transition with hysteresis.

All the three samples show a marked change of colour from pink in the LS state of Fe^{2+} to white in the HS state of this ion. The thermochromic effect has been followed with a simple optical transmission device [12] through the temperature range of the spin transition[1]. By definition, the spin transition temperatures in the warming and cooling modes, $T_{1/2}\nearrow$ and $T_{1/2}\swarrow$, correspond to $x = 0.5$.

[1] The authors are grateful to L. Sommier from the Laboratory of O. Kahn (Laboratoire des Sciences Moléculaires, Institut de Chimie de la Matière Condensée de Bordeaux, 33608 Pessac Cedex, France) for carrying out the optical measurements.

The transition temperatures deduced from the DSC curves are in fairly good agreement with those obtained by optical reflectivity, see Table 4. The enthalpy variations (in the warming mode) determined from the DSC are also given in Table 4. The corresponding entropy variations are calculated as $\Delta S = \Delta H/T_{1/2}\nearrow$.

The experimental hysteresis curves deduced from the optical reflectivity data have been fitted to by theoretical $x(T)$ graphs, as shown in Figure 8. The fitting results in the interaction energies and numbers of ions per domain shown in Table 4.

The electron paramagnetic resonance (EPR) spectra were recorded with an X-band (9.3 GHz) Varian V4502 spectrometer equipped with a Varian E257 variable temperature accessory operating in the range 88 to 573 K. Figure 9 shows the EPR spectra in the temperature range of the spin transition for 10% Cu/Fe-containing samples of $[Fe(Htrz)_2trz)](BF_4)$ and of an analogous compound $[Fe(NH_2trz)_3](NO_3)_2$. In the warming mode, as far as the temperature remains lower than $T_{1/2}\nearrow$, (the LS state of Fe^{2+} ions) the EPR spectra in both systems exhibit a signal from Cu^{2+} ions with poorly resolved hyperfine splitting. Above $T_{1/2}\nearrow$ (the HS state of Fe^{2+}) a severe change occurs in the aspect of the EPR spectrum of $[Fe_{0.9}Cu_{0.1}(Htrz)_2(trz)](BF_4)$ and the spectrum totally disappears in the case of $[Fe_{0.9}Cu_{0.1}(NH_2trz)_3](NO_3)_2$. In the cooling mode, as the temperature decreases below $T_{1/2}\swarrow$, the initial EPR spectra shapes are approximately restored.

In the context of the present study, of most interest are the EPR manifestations of the domain structure which will be discussed in Section 5.3.

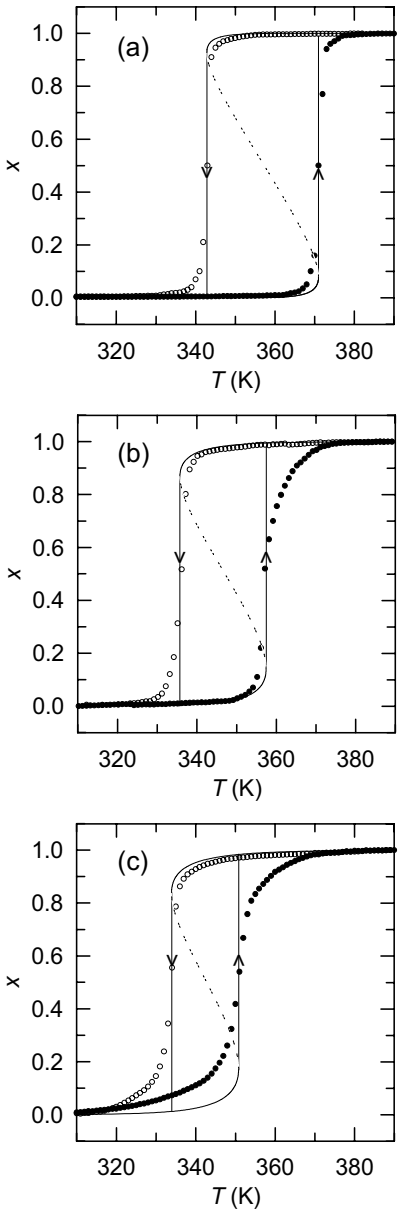

Fig. 8. Computer fitting to the optical transmission data in the warming (•) and cooling (∘) modes. The dashed line represents the physically inaccessible states. The simulation parameters are reported in Table 4 for $y = 0.00$ (a), $y = 0.01$ (b) and $y = 0.10$ (c).

5 Discussion

5.1 Theoretical model

The thermodynamic models taking into account non-interacting domains of like-spin ions cannot explain hysteresis effects [9]. On the other hand, the regular solution model that does not take into consideration the existence of domains, cannot describe the square-shaped hysteresis loops as sometimes experimentally observed. In contrast, the interacting domain model explains in quite a satisfactory way the behaviour of spin conversion systems in the cases of both gradual and abrupt transitions with hysteresis. The interacting domain model shows that abruptness and completeness of the spin transition rapidly grow with the domain size, see Figures 5 and 6. These predictions are in conformity with the experimental observations (see next section).

In the framework of the regular solution model of spin conversion [8], Slichter and Drickamer have suggested the inequality $\Gamma > 2RT_{1/2}$ to be the necessary and sufficient condition of the existence of hysteresis. Yet, it is clear from the present model that this condition must be modified. Indeed, the point P defined in Section 2.2 belongs to the regions III or IV, if and only if the following inequalities hold:

$$2rT_{1/2} < \Gamma < \Delta H \coth(\Delta S/2r). \tag{21}$$

In the $n = 1$ case, tantamount to the regular solution model from the mathematical standpoint, r must be replaced by the perfect gas constant $R = \mathcal{N}k_{\mathrm{B}}$, so that one gets

$$2RT_{1/2} < \Gamma < \Delta H \coth(\Delta S/2R). \tag{22}$$

It can be concluded that there exists not only a lower limit but also an upper limit of the Γ values, therefore, the hysteresis loop vanishes for both weak and very strong interactions between domains (or individual ions). In the latter case, if thermal fluctuations and tunnelling through the free energy barrier are negligible, the thermodynamic system is bound to indefinitely remain trapped in a metastable HS state (region V).

The *sine qua non* condition of hysteresis is the existence of a maximum of the $G_T(x)$ function, separating two distinct minima and constituting an energy barrier usually considered as impenetrable [13]. On the other hand, if one takes into consideration the possibility for certain ions to get sufficient energy to overcome this barrier, the hysteresis loop will be narrowed and made less abrupt. As the probability of thermally activated "jumping" over the barrier is expected to be temperature-dependent, such a mechanism would bring about a pronounced asymmetry of the hysteresis loop that would become more abrupt in the cooling mode than in the warming mode. However, the experimental hysteresis curve in the $[Fe(Htrz)_2trz](BF_4)$ compound does not show such an asymmetry, see Figure 8a. This gives one more evidence of the fact that the spin transition occurs in domains of like spins. Indeed, the probability for a whole domain to overcome the energy barrier between the local and the global free-energy minima must very rapidly decrease with the increasing number of ions per domain.

The possibility of "inhabitual" irreversible spin transitions in the regions II, IV and V constitutes perhaps the most interesting result of the present analysis.

In the regions II and IV, if at low temperature the system initially is in the metastable HS state, an irreversible HS to LS transition will occur at a temperature below the onset of a usual, reversible LS to HS transition. If such excited HS state can effectively be populated

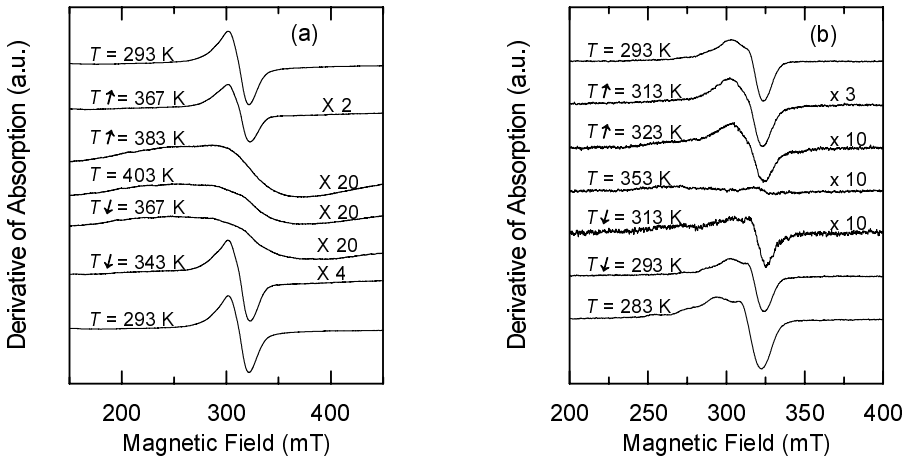

Fig. 9. EPR spectra in the spin transition region in the warming ($T \nearrow$) and cooling ($T \swarrow$) modes for the $[Fe_{0.9}Cu_{0.1}(Htrz)_2(trz)](BF_4)$ (a) and $[Fe_{0.9}Cu_{0.1}(NH_2trz)_3](NO_3)_2$ (b) polymeric compounds.

by light, the LIESST effect would be observed. The experimental observation of this effect has been reported in some spin transition compounds [14,15]. One might wonder why the possibility of the low-temperature metastable HS state had not been discussed in the previous publications concerned with the thermodynamic models of the spin conversion, *e.g.* [8,11], since it can be inferred in a straightforward way from equation (14). Most probably, the answer is that the possible experimental application of such a state, the LIESST effect, had not yet been known at that time.

In the region V, as discussed above, only an irreversible spin transition can take place. Note that the HS state trapping has been experimentally observed in $Fe(stpy)_4(NCS)_2$ compound by inducing a *trans-cis* ligand phototransformation [16].

We have already mentioned that in the present model metastable states have infinitely long (geological) lifetimes. In the experimental LIESST studies of $[Fe(ptz)_6](BF_4)_2$ compound the lifetime of the metastable HS states at 10 K is about 40 days [17]. Only at temperatures as high as *ca.* 50 K the thermal relaxation back to the stable LS state begins to set in. In the spin-crossover solid solution $[Fe_xCo_{1-x}(btr)_2(NCS)_2]H_2O$ relatively short and strongly temperature-dependent decay times of the metastable HS state are observed [18], however, no data has been reported for temperatures lower than 45 K. On the other hand, very slow relaxation of the metastable low-temperature HS state is found in $[Fe(PM-BiA)_2](NCS)_2$ compound, namely, at 50 K no obvious decrease of the HS fraction at all is detected on the time scale of several thousands of seconds. The low-temperature lifetime limit can be estimated as about 1 year in this case [19]. Thus, it seems that the infinite lifetime approximation is not in contradiction with experimental LIESST observations, at least, at sufficiently low temperatures.

This extraordinary stability of the low-temperature HS state can be related to the difference Δr in the average iron-to-ligand bond length between the two spin states [17]. More precisely, as Δr is increased, the pre-exponential (tunneling) factor in the spin conversion rate expression decreases very rapidly. For $[Fe(ptz)_6](BF_4)_2$ $\Delta r \approx 0.18$ Å, while for $[Fe(PM-BiA)_2](NCS)_2$ an unusually large value of $\Delta r \approx 0.27$ Å has been found.

5.2 Effect of copper on the spin transition in $[Fe(Htrz)_2trz](BF_4)$

The occurrence of abrupt transition with hysteresis is related to cooperativity. Although its mechanism is not yet fully understood, it is commonly accepted that cooperative interactions become extremely important when the active spin-changing sites are covalently linked by conjugated ligands [2]. The EXAFS data suggest for the $[Fe(Htrz)_2trz](BF_4)$ molecular compound a basic structure of a linear chain in which two adjacent ferrous ions are triply bridged by two triazole ligands and one deprotonated triozalato ligand through the 1, 2 nitrogen positions [20]. So the large interaction energy, $\Gamma = 2.010\ \mathrm{kJ\,mol^{-1}}$, deduced for the $y = 0.00$ compound, see Table 4, is not surprising.

It is well known that in undoped compounds, the cooperativity manifests itself at longer distances than in doped compounds. In the first case, the size of the like-spin domains is likely to be limited by crystal imperfections and local stresses [21]. Foreign ions introduced into a spin transition polymer constitute an additional natural boundary between domains, thus further reducing their size and consequently reducing the steepness of the spin conversion. Indeed, in $[Fe_{1-y}Cu_y(Htrz)_2trz](BF_4)$ the average domain size decreases from $n = 11$ for $y = 0.00$ to $n = 6$ for $y = 0.10$, see Table 4. The experimental data presented in Table 4 show a tendency of Γ to increase as the size of domains is increased. This is in contrast to the behaviour expected for negligible interchain interactions, see equation (11) and Figure 5. Note that recent Wide-Angle X-ray Scattering (WAXS) data suggest the possibility of connecting the polymer chains through hydrogen

bonds between the BF_4^- anions [22]. However, an *increase* of Γ with the increase of n can only be explained by a relatively strong increase in the interdomain interaction energies.

Another effect of doping the spin compound is a pronounced shift of the transition temperatures. It can be understood on the basis of the effective ionic radii. The octahedral radius of the Cu^{2+} ion, 0.73 Å, is larger than the corresponding radii of Fe^{2+} in the LS state, 0.63 Å, so, the presence of copper seems to favour the HS state of Fe^{2+} at the expense of its LS state. Consequently, one needs less warming to bring about the LS to HS transition and more cooling to produce the HS to LS back transition, so that all the characteristic transition temperatures in the copper-containing compounds are lowered. One more manifestation of the copper-favoured HS state of Fe^{2+} ions is the more important "residual paramagnetism" in the LS state of these ions, see Figure 8. The residual molar HS fraction just before the abrupt stage of the LS to HS transition can be evaluated from the best-fit hysteresis curves as 0.08, 0.142 and 0.174, respectively for the $y = 0.00, 0.01$ and 0.10 compounds.

5.3 EPR manifestations of the presence of domains

A more detailed inspection of the EPR spectra in $[Fe_{0.9}Cu_{0.1}(Htrz)_2(trz)](BF_4)$ in the spin transition region, see Figure 9a, reveals the presence of two superposed components, a narrower one and a broader one. One might suggest that what actually takes place in the course of the spin transition is not a *broadening* of the spectral features, but rather a *decrease* of the amplitude of the Cu^{2+} EPR spectrum corresponding to the LS state of Fe^{2+} (the narrow component) which is gradually replaced by a broader component corresponding to the HS state of Fe^{2+}. Such a behaviour can be explained by the fact that the Cu^{2+} ions are located inside LS or HS Fe^{2+} ion domains. In this event, most of Cu^{2+} ions are predominantly surrounded either with LS or with HS Fe^{2+} ions.

This behaviour is still more pronounced in the $[Fe_{0.9}Cu_{0.1}(NH_2trz)_3](NO_3)_2$ compound, see Figure 9b, in which case the Cu^{2+} EPR spectra in the HS state of Fe^{2+} are broadened beyond the possibility of observation at the X-band. It is obvious from Figure 9b that in the spin transition region the EPR spectra of Cu^{2+} gradually disappear, without any appreciable broadening.

On the other hand, if in the spin transition region the LS and HS Fe^{2+} ions were dispersed at random, a gradual transformation of the EPR spectra of a paramagnetic probe would be observed, which is clearly not the case. Thus, the EPR data confirm a coexistence of LS and HS Fe^{2+} domains in the spin transition region.

Note that still more spectacular manifestations of the presence of like-spin domains have been observed for ferrous compounds presenting well-resolved EPR spectra of Mn^{2+} ions, $[Fe(2\text{-pic})_3]Cl_2C_2H_5OH$ and $Fe(PM\text{–}PEA)_2(NCS)_2$ [23,24]. In these cases the EPR spectra in the transition region have been shown to consist of superpositions of two distinct signals corresponding to the Mn^{2+} ions surrounded with either only HS or only LS Fe^{2+} ions. Similar conclusions have been reached by nuclear magnetic resonance technique [25].

Another interesting implication of the EPR data in the $[Fe_{0.9}Cu_{0.1}(Htrz)_2(trz)](BF_4)$ polymer concerns the effective g-value of the Cu^{2+} signal in the HS state of Fe^{2+}, $g_{\text{eff}} = 2.05$, which is quite different from the *mean* g-value of the Cu^{2+} spectrum in the LS state of Fe^{2+}, $\langle g \rangle = \frac{1}{3}(g_x + g_y + g_z) \approx 2.15$. This distinction suggests that the LS to HS conversion is accompanied by a structural transition (twisting of polymer chains), as has been corroborated by the WAXS measurements [22]. Such a transformation results in an enhanced cooperativity and contributes to stabilising the new spin state. This finding is in agreement with the general idea of discontinuous spin transitions being associated with a crystallographic phase change [26].

6 Conclusion

Introducing the hypothesis that spin-changing ions in a metal-organic polymer form interacting like-spin domains of equal size results in a generalisation of the Slichter-Drickamer model. Computer simulations demonstrate that the position and shape of spin conversion curves are very sensitive to the thermodynamic parameters ΔH, ΔS and Γ. Namely, concerning the hysteresis loop, its abruptness, completeness and width may transform themselves in a very different way with the domain size, n, depending on the form of $\Gamma(n)$. Besides, it has been shown that the hysteresis loop vanishes not only for weak interactions but also for very strong interactions between domains or individual ions.

The low-temperature bistability due to a strong cooperativity of spin-changing units has been examined here for the first time. This bistability may result in two different kinds of irreversible spin transitions that occur if the spin system at low temperatures remains trapped in a metastable HS state. The possibility of optically populating such states by the LIESST effect is particularly interesting since it may result in very long decay times.

The model can be readily generalised to two or three-dimensional lattices by introducing the interaction energy in a phenomenological way.

Experimental spin transition studies, carried out for copper-containing ferrous polymer compound $[Fe_{1-y}Cu_y\ (Htrz)_2trz](BF_4)$ by DSC and optical transmission have been convincingly fitted to by the interacting domain model. In particular, a correlation has been found between Γ and n suggesting that the interdomain interaction energies increase with the increase in the domain size.

The EPR data give further evidence of coexistence of LS and HS Fe^{2+} domains in the spin transition region. On can see from the above analysis that the EPR technique in certain cases may be sensitive not only to the coordination polyhedron of a paramagnetic ion but also to the structure of more remote environment.

In its present form, the interacting domain model is certainly oversimplified. Its further developments must take into account a possibility of different sizes of LS and HS domains and, more generally, a possibility of statistical distributions of the domain sizes. Besides, temperature dependence of the domain size and interdomain interaction energies can be taken into account, which may prove necessary especially in the case of a spin conversion spread over a large temperature range. The dependence of the transition cooperativity on the domain size may be described in detail in the framework of a microscopic theory.

Finally, we note that the interacting domain model can be extended, *mutatis mutandis*, to first order phase transitions.

The authors are indebted to O. Kahn for synthesis of the spin transition polymers and valuable discussions.

References

1. P. Gütlich, A. Hauser, H. Spiering, Angew. Chem. Int. Ed. Engl. **33**, 2024 (1994).
2. O. Kahn, C. Jay, Science **279**, 44 (1998).
3. O. Kahn, *Molecular Magnetism* (VCH Publishers, Inc., New-York, 1993), p. 67.
4. J. Zarembowitch, New J. Chem. **16**, 255 (1992).
5. M. Haddad, W.D. Federer, M.W. Lynch, D.N. Hendrickson, Inorg. Chem. **279**, 131 (1981).
6. P. Gütlich, H. Köppen, R. Link, H.G. Steinhäuser, J. Chem. Phys. **70**, 3977 (1979).
7. R. Zimmermann, E. König, J. Phys. Chem. Solids **38**, 779 (1977).
8. C.P. Slichter, H.G. Drickamer, J. Chem. Phys. **56**, 2142 (1972).
9. H. Sorai, S. Seki, J. Chem. Phys. Solids **35**, 555 (1974).
10. E. König, B. Kanellakopulos, B. Powietzka, H.A. Goodwin, Inorg. Chem. **29**, 4944 (1990).
11. K.F. Purcell, M.F. Edwards, Inorg. Chem. **23**, 2620 (1984).
12. O. Kahn, E. Codjovi, Phil. Trans. Royal Soc. London Ser. A **354**, 359 (1996).
13. R. Zimmermann, J. Phys. Chem. Solids **44**, 151 (1983).
14. S. Descurtins, P. Gütlich, K.M. Hasselbach, A. Hauser, H. Spiering, Inorg. Chem. **24**, 2174 (1985).
15. J.F. Létard, P. Guionneau, L. Rabardel, J.A.K. Howard, A.E. Goeta, D. Chasseau, O. Kahn, Inorg. Chem. **37**, 4432 (1998).
16. C. Roux, J. Zarembowitch, B. Gallois, T. Granier, R. Claude, Inorg. Chem. **33**, 2273 (1994).
17. P. Gütlich, A. Hauser, H. Spiering, Angew. Chem. Int. Ed. Engl. **33**, 2024 (1994).
18. A. Desaix, O. Roubeau, J. Jeftic, J.G. Haasnoot, K. Boukheddaden, E. Codjovi, J. Linarès, M. Noguès, F. Varret, Eur. Phys. J. B **6**, 183 (1998).
19. J.-F. Létard, H. Daubric, C. Cantin, J. Kliava, Y.A. Bouhedja, O. Nguyen, O. Kahn, Mol. Cryst. Liq. Cryst. **335**, 1207 (1999).
20. J. Krober, J.P. Audière, R. Claude, E. Codjovi, O. Kahn, Chem. Mater. **6**, 1404 (1994).
21. E. König, G. Ritter, S.K. Kulshreshtha, Chem. Rev. **85**, 219 (1985).
22. M. Verelst, L. Sommier, P. Lecante, A. Mosset, O. Kahn, Chem. Mater. **10**, 980 (1998).
23. P.E. Doan, B.R. Mc.Garvey, Inorg. Chem. **29**, 874 (1990).
24. H. Daubric, C. Cantin, C. Thomas, J. Kliava, J.-F. Létard, O. Kahn, Chem. Phys. **244**, 75 (1999).
25. A. Ozarowski, Y. Shunzhong, B.R. McGarvey, A. Mislankar, J.E. Drake, Inorg. Chem. **30**, 3167 (1991).
26. E. König, Prog. Inorg. Chem. **35**, 527 (1987).